Earth and Planetary Science Letters 452 (2016) 227–237

Contents lists available at ScienceDirect

Earth and Planetary Science Letters

www.elsevier.com/locate/epsl

Titanium-hydroxyl defect-controlled rheology of the Earth's upper mantle

Ulrich H. Faul [a,b,*], Christopher J. Cline II [b], Emmanuel C. David [b,1], Andrew J. Berry [b], Ian Jackson [b]

[a] Earth Atmospheric and Planetary Sciences, Massachusetts Institute of Technology, Cambridge, MA, USA
[b] Research School of Earth Sciences, Australian National University, Canberra, Australia

ARTICLE INFO

Article history:
Received 11 February 2016
Received in revised form 7 June 2016
Accepted 10 July 2016
Available online 18 August 2016
Editor: B. Buffett

Keywords:
upper mantle
deformation
olivine
water
defects
FTIR spectroscopy

ABSTRACT

Experiments were conducted with hydrous olivine to investigate the defect responsible for the influence of water (hydrogen structurally incorporated as hydroxyl) on the olivine rheology. Solution–gelation derived Fo_{90} olivine doped with nominally 0.04–0.1 wt.% TiO_2 was first hot-pressed and then deformed in platinum capsules at 300 MPa confining pressure and temperatures from 1200–1350 °C. The water content was not buffered so that deformation occurred at water-undersaturated conditions. Due to the enhanced grain growth under hydrous conditions, the samples were at least a factor of three more coarse-grained than their dry counterparts and deformed in powerlaw creep at differential stresses as low as a few tens of MPa. Since all experiments were conducted at the same confining pressure, the essentially linear relationship between strain rate and water content was for the first time determined independently of an activation volume. Infrared spectra are dominated by absorption bands at 3572 and 3525 cm^{-1}. These bands also predominate in infrared spectra of natural olivine, and can only be reproduced experimentally in the presence of titanium. In contrast to the previous interpretation of the hydrous rheology in terms of intrinsic point defects, the experiments show that extrinsic defects (impurities) in natural olivine play the dominant role for water weakening at the water contents expected for most of the upper mantle.

1. Introduction

It is well established that olivine deformed in the presence of water is weaker than when deformed under dry conditions (Avé Lallemant and Carter, 1970; Chopra and Paterson, 1984; Mackwell et al., 1985; Karato et al., 1986; Mei and Kohlstedt, 2000a, 2000b). These studies confirmed a relationship between the presence of water and strength, but because experiments were always carried out under water-saturated conditions the relationship between water fugacity and strength were not determined independently of confining pressures (Hirth and Kohlstedt, 2003; Karato and Jung, 2003).

Less clear is the point defect mechanism for weakening due to water. Fits to experiments at a range of pressures yielded a relationship between strain rate and water fugacity (fH_2O) with an exponent r as $\dot{\epsilon} \propto fH_2O^r$. Models of point defects were then examined to obtain the same exponent through a combination of the dominant defect for charge neutrality and diffusive accommodation of strain (Karato, 1989a; Mei and Kohlstedt, 2000a, 2000b). The hydrous defects thus inferred can not be readily reconciled with infrared absorption spectra from experiments aimed at correlating absorption bands with particular defects (Matveev et al., 2001; Lemaire et al., 2004; Berry et al., 2005). The defect models for deformation considered only intrinsic defects (vacancy and interstitial O, Mg, Fe^{2+}, Si, Fe^{3+} on octahedral and tetrahedral sites, and electrons, Kohlstedt and Mackwell (1998)). By contrast, natural olivine contains a range of impurities with abundances in the ppm range (extrinsic defects, de Hoog et al. (2010), Foley et al. (2013)). Previous experiments showed that titanium is required to experimentally reproduce the infrared spectra typical of natural samples (Berry et al., 2005). Ab inito modelling indicated that the associated hydrous defect is the most stable defect, potentially affecting the strength of olivine (Walker et al., 2007).

The experiments described in the following were carried out with Ti-doped olivine to investigate the role of this impurity on the rheology under hydrous conditions. The use of Pt capsules and $Ni_{70}Fe_{30}$ foils permitted water retention at a range of water contents at fixed confining pressure. The experiments were con-

* Corresponding author.
E-mail address: hufaul@mit.edu (U.H. Faul).
[1] Now at: Department of Earth Sciences, University College London, London, UK.

http://dx.doi.org/10.1016/j.epsl.2016.07.016
0012-821X/

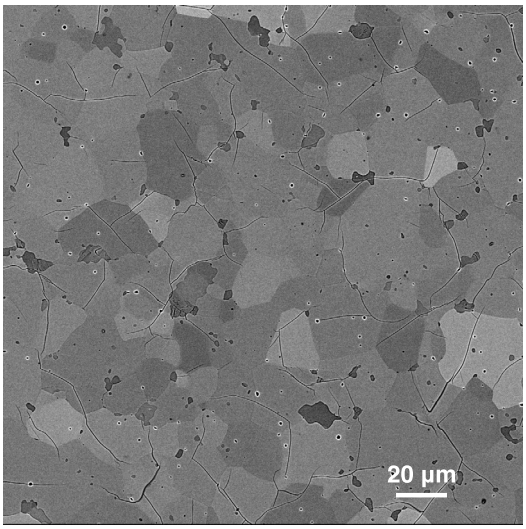

Fig. 1. Representative scanning electron microscope backscattered-electron image of the microstructure after hotpressing (prior to deformation). The grayscale variation of olivine crystals is due to orientation contrast. Darker patches predominantly on olivine grain boundaries and corners are orthopyroxene grains. Small orthopyroxene grains are also incorporated into olivine during growth from an estimated grain size of 1 μm prior to hotpressing. Cracks originate during cooling due to the thermal expansion anisotropy of olivine. Small pores inside olivine grains stand out due to their bright rim.

ducted at water-undersaturated conditions corresponding to those for most of the upper mantle. Infrared spectra were used to determine the water content and identify the hydrous defect associated with the observed water weakening.

2. Sample materials and experimental setup

The starting materials for the experiments were prepared by a solution–gelation process, resulting in fine-grained, chemically pure and homogeneous precursors (Faul and Jackson, 2007). For this study, Ti was added as tetra-ethoxy orthotitanate (TEOT, Berry et al., 2007b). The amount of Si in the gel was in excess of stoichiometric olivine (Fo_{90}) composition to ensure Si saturation (Fig. 1). After drying of the solution, the raw powders were reacted at 875 °C and repeatedly fired at 1200 °C and an fO_2 near the CCO buffer for more than 12 h. The powders were cold pressed into pellets that were again fired at an fO_2 near the CCO buffer and kept in a drying oven until wrapping in ∼70 μm thick $Ni_{70}Fe_{30}$ foil (with nominally either 0.04 or 0.1 wt.% TiO_2 added) or encapsulation in laser-welded Pt capsules (0.04 wt.% TiO_2 added, with a foil thickness of 180 μm and 250 μm for hotpressing and deformation experiments, respectively). Table 1 provides a summary of experimental conditions and compositions. Each wrapped/encapsulated sample was inserted in a mild steel jacket and hot-pressed for 24 h at the same temperature as the subsequent deformation experiment. The temperature uncertainty is estimated as ±10 °C from regular furnace calibrations. All experiments were carried out at a confining pressure of 300 MPa.

After hot-pressing, the jacket was dissolved in acid, the Pt capsule peeled off and a ∼1 mm thick slice was sectioned about 1.5 mm from the top end of the sample for microstructural examination and Fourier transform infrared (FTIR) spectroscopy. Each fully dense sample was precision ground to a cylinder with a diameter of 11.5 mm and a lengths near 25 mm before being re-fired at CCO and 1200 °C for 12 h prior to re-encapsulation for deformation. The deformation experiments were carried out in a gas medium (Paterson) apparatus under triaxial compression in a pre-programmed sequence of constant load segments, with load increasing after each segment. The load (force) was measured internally, displacements externally. Further details on the apparatus calibration and deformation procedures are given in Faul and Jackson (2007). After deformation a horizontal slice about 1 mm thick and 1.5 mm from the top or bottom end of each sample was prepared for microstructural and analytical examination.

The total strain for samples 6652 and 6656 with 0.1 wt.% Ti and deformed in $Ni_{70}Fe_{30}$ foils after the first 'staircase' of constant load was relatively small. Therefore, the load was reduced to zero and a second pass was programmed. This second pass provides a measure of the reproducibility of the strain rates. Similarly, 6795 with modest total strain was deformed again as 6803 after precision grinding to 10 mm diameter and 20 mm length, firing at 1200 °C at CCO conditions and re-encapsulation in Pt. Samples that were deformed to relatively high strains (6767 and 6803) began to flow around the pistons at both ends. In some instances canting was observed as a consequence of deformation.

3. Analytical methods

The samples were examined optically, by scanning electron microscopy (SEM), electron back-scatter diffraction (EBSD), electron probe micro-analysis (EPMA), laser ablation inductively coupled mass spectrometry (LA-ICPMS) and FTIR spectroscopy. Imaging and EBSD mapping were performed using a Zeiss Ultra Plus field emission scanning electron microscope at the Center for Advanced Microscopy at ANU. The EBSD maps were collected with an Oxford Instruments camera and HKL software from carbon coated samples at 20 kV acceleration voltage and 5 nA beam current. The maps consist of 400 × 400 or 450 × 450 points with indexing rates usually near 80%. The maps were processed with MTEX software. The grain sizes were determined from the EBSD maps as the equivalent diameter of a circle with the same area of each grain in the map. A sectioning correction factor of $4/\pi$ was applied to obtain the mean diameters in Table 1.

Microprobe analyses were performed using the CAMECA SX100 microprobe at RSES, ANU on selected samples to determine the Mg# (the molar ratio $100 \times Mg^{2+}/(Mg^{2+} + Fe^{2+})$). LA-ICPMS was performed at RSES ANU with an Excimer laser and a single collector mass spectrometer (Agilent 7700) with a spot size of 70 μm to determine the Ti contents in olivine given in Table 1. We also analysed a NIST 610 glass as a standard.

FTIR spectroscopy and the determination of the water content are detailed in Appendix A. Briefly, we measured the absorbance on 400 micron thick sections to enable measurements even at low water contents. Molecular water and hydroxyl contents were determined separately from the spectra. For the hydroxyl content we used the site-specific absorption coefficient from Kovacs et al. (2010), which is similar to the coefficient of Bell et al. (2003). The water content given in Table 1 is averaged from 25–30 measurements on radial traverses.

4. Results

4.1. Composition, microstructure and water content

After hotpressing, the samples are characterised by a near ideal 'foam' microstructure (Fig. 2a) with equant crystalline grains and a relatively narrow grain size distribution (Fig. 3, left). Orthopyroxene, derived from the excess silica in the gel as well as from grinding of the powders in agate mortars, is relatively homogeneously distributed as small grains located frequently at olivine grain corners (Fig. 1). Grain growth rates for water-bearing samples are significantly faster than for dry samples (Table 1, Karato, 1989b), with growth rates modulated by the orthopyroxene grains. Grains with non-uniform orientation (coloured in Fig. 2a) indicate coalescence of neighbours.